Supplementary Information (SI) for Lab on a Chip.
This journal is © The Royal Society of Chemistry 2025

Supplementary Information

Densimeter-on-Chip (DoC): measuring a single-cell mass density by sedimentation in microchannel flows

David Dannhauser,* [a,†] Maria Isabella Maremonti,[a,†] Paolo Antonio Netti[a,b] and Filippo Causa[a]

[a] Interdisciplinary Research Centre on Biomaterials (CRIB) and Dipartimento di Ingegneria Chimica, dei Materiali e della Produzione Industriale, University of Naples "Federico II", 80125 Naples, ITALY.
[b] Center for Advanced Biomaterials for Healthcare@CRIB, Istituto Italiano di Tecnologia, 80125 Naples, ITALY.
† The authors contributed equally.

Governing equation and alignment condition

To compute the velocity and stress profiles in our microfluidic chip, we fixed a cartesian reference frame, denoting with x the flow direction, y the neutral direction and z the gradient direction, orthogonal to the plates. By assuming incompressibility and neglecting any inertia term of the medium, the governing equations for the problem are[1]:

$$\nabla \cdot \bar{\sigma} = 0, \tag{1}$$

$$\nabla \cdot u = 0, \tag{2}$$

$$\bar{\sigma} = -p\bar{I} + 2\eta_S \bar{D} + \bar{\tau}, \tag{3}$$

defined as the momentum balance, the continuity equation, and the fluid stress tensor expression, respectively. Hereby, $\bar{\sigma}$, u, p, $\bar{I}$, η_S, $\bar{D}$, are stress tensor, velocity vector, pressure, unity tensor, solvent Newtonian viscosity, and rate-of-deformation tensor, respectively. Moreover, the viscoelastic stress tensor can be specified by the Giesekus equation model [2]:

$$\lambda \bar{\tau}_{(1)} + \bar{\tau} + \frac{\alpha\lambda}{\eta_P}\bar{\tau} \cdot \bar{\tau} = 2\eta_P \bar{D} \tag{4}$$

where λ is the relaxation time of the fluid, η_P is the polymer viscosity and $\bar{\tau}_{(1)}$ is the upper-convected time derivative, expressed as:

$$\bar{\tau}_{(1)} = \frac{D}{Dt}\bar{\tau} - \{\bar{\tau} \cdot \nabla u\}^T - \{\bar{\tau} \cdot \nabla u\} \tag{5}$$

The non-dimensional parameter α defines the shear-thinning behaviour of the viscoelastic fluid if greater than 0. When α goes to zero, the fluid has a constant viscosity and the Giesekus constitutive equation degenerates into the Oldroyd-B model[2],

$$\lambda \bar{\tau}_{(1)} + \bar{\tau} = 2\eta_P \bar{D} \tag{6}$$

The overall zero-shear viscosity (η_0) for the Oldroyd-B fluid model, as well as for the Giesekus one, is given by the summation of the solvent and the polymer viscosity contributions,

$$\eta_0 = \eta_S + \eta_P \tag{7}$$

In this work, we choose to model the viscoelastic medium by the Oldroyd-B constitutive equation. Furthermore, the fluid flow conditions have been analysed by using dimensionless numbers, imposing the channel height (H) as characteristic length. Thus, the most relevant non-dimensional geometrical channel design parameters are the blockage ratio (β) and the aspect ratio of the channel section ($AR_{Channel}$):

$$\beta = d_1/H,$$

$$AR_{Channel} = W/H \geq 2,$$

with d_1 the cell diameter and W the channel width. The fluid-flow condition can be modelled by:

$$Re = \rho \bar{U} D_h / \eta_0,$$
$$Wi = 2\lambda \bar{U} / H,$$
$$El = Wi/Re,$$

the Reynolds (Re), Weissenberg (Wi) and Elasticity (El) numbers, respectively. We can further recall ρ as the fluid density, U as the average fluid velocity, D_h the characteristic hydraulic diameter of a capillary or duct. In other words, Wi defines the product between characteristic time scale of the fluid flow and time scale of the material fluid, Re relates inertial and viscous components of the fluid flow condition, while El, defines the importance of inertial components with respect to elastic ones.[3]

Further, keeping in mind that Wi has to be around 1, we set all of the fluid flow conditions in order to have $Wi \gg Re$ and therefore $Re \ll 1$, avoiding any inertial and vortex contribution to the flow conditions.[4] Moreover, cells are assumed to generate no flow disturbances, which can be confirmed by cell Re ($Re_{cell} = \beta Re$), defined as a scaling version of the one of the viscoelastic fluid -with remaining $Re \ll 1$ condition- avoiding turbulences and fluid flow alterations.[5]

In the hypothesis of an applied pressure-driven flow, the inlet pressure (ΔP) is scaled with respect to the hydraulic resistances of each cross-section, computed with respect to the series and/or parallel disposition of the channel sections, as reported:

$$\Delta P = R_{Eq} Q \tag{8}$$

where, from the device design:

$$R_{Eq} = R_{Inlet} + R_{Channel} + (R_{Exit1} * R_{Exit2})/(R_{Exit1} + R_{Exit2}) \tag{9}$$

and

$$R_{Inlet} = R_{Exit_i} = \frac{8}{\pi} \eta L_{Inlet\ or\ Exit_i} \frac{1}{\left(\frac{D_{Inlet\ or\ Exit_i}}{2}\right)^4} \tag{10}$$

$$R_{Channel} = \frac{12 \eta L_{Channel}}{1 - (H/W) 0.63} \frac{1}{W H^3} \tag{11}$$

R_{Cap} and $R_{Channel}$ are the hydraulic resistances for the capillary and rectangular cross-sections.[6] The subscripts stand for the different inlet and exits regions present along the microfluidic device (Scheme 1 and Fig. S3) since they are all circular and then the hydraulic resistance expression is the same.

Cell alignment and/or deformation conditions are considerate with the following assumptions. Spherical objects migrate in the direction of minimum shear rates ($\dot{\gamma}$) for a Poiseuille flow. In fact, lateral gradients of normal stresses in the full velocity field are responsible for the migration observed in viscoelastic fluids.[7] The non-deformed object will follow the fluid velocity along a constant direction (maximum velocity for the Poiseuille flow) minimizing perturbations caused by the object itself.[8,9] The viscoelastic stress and force will assume different profiles depending on the channel geometry (circular or rectangular). In general, for a steady-state Poiseuille flow, we can write a simple force balance in the direction of the shear gradient. Forces are balanced at the equilibrium flow positions of the particle (centre line for a tube and both central axis and corners for a duct).[3,8]

We consider elastic forces only in gradient direction (z-axis) with H<<W, expressed as,[3,4]

$$F_E \propto C \left(\frac{d_1}{2}\right)^3 \nabla N_1, \tag{12}$$

being proportional to the gradient of the first positive normal stress difference ($N_1 = 2\lambda \eta_0 \dot{\gamma}^2$). C is a non-dimensional parameter, defined with respect to the chosen fluid.[1]

In general, for viscoelastic alignment purposes, with a negligible inertia F_E can be balanced with Stokes drag () expressed as:

$$F_D = 0.5 \rho U_S^2 {C_D}^{-1} A \tag{13}$$

where A and ρ are the particle area and density, respectively.
Finally, we verified if the following relationships is satisfied for the in-flow viscoelastic alignment:

$$\Theta = A_P Wi\beta^2 \frac{L}{H} > -ln(3.5\beta) \quad (14)$$

with A_P a channel geometry constant and L the minimum length needed to observe a stable centre-line alignment.[8,10] We specified A_p starting from the Poiseuille profile, resulting in 3 and 1.5 for capillary and rectangular geometries, respectively.[11]

Sedimentation velocity and falling length computation

If particles fall, the applied force balance can be rewritten as:

$$F_{Ez} + F_G - F_{Dz} - F_B = m_p \frac{dU_S}{dt}$$

where velocity and position vary in z-direction. m_p is the particle mass that can be expressed also as the product of the particle density and particle volume:

$$m_p = V_p \rho_p$$

The initial condition on the velocity is given by:

$$t = 0 \qquad U_0 = U_{max}$$

U_0 is different from 0 since we are assuming that the particles are aligned at the centre line of the channel, at $H/2$. The buoyant force $F_g - F_b$ can be expressed as a function of the fluid (ρ_f) and particle densities. Then, the balance becomes:

$$Ca^3 \nabla N_1 + \frac{4}{3}\pi a^3(\rho_p - \rho_f)g - 6\pi\eta a\left(1 - \frac{9}{32}\left(\frac{1}{\zeta}\right)\right)^{-1} U_{Sz} = \rho_p V_p \frac{dU_S}{dt}$$

The solution is:

$$U_{Sz}(t) = \left[U_{max} e^{-\frac{6\pi a\eta}{\rho_p V_p}t} + \frac{Ca^3 \nabla N_1 \rho_p V_p}{\rho_p V_p \; 6\pi a}\left(1 - e^{-\frac{6\pi\eta a}{\rho_p V_p}t}\right)\right]\left(1 - \frac{9}{32}\left(\frac{1}{\zeta}\right)\right) \quad (15)$$

where the ratio $6\pi\eta a/\rho_p V_p$ is the inverse of the time constant of the process. Since this time is small enough (~µs) compared to the fluid-flow time (~s), we can assume that it is negligible.

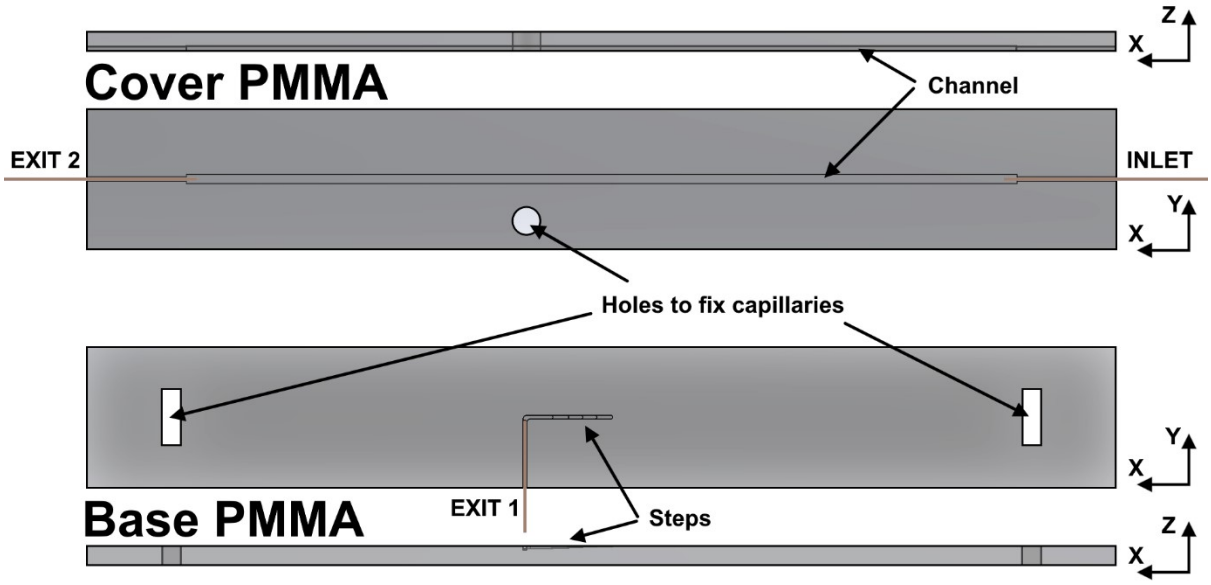

Fig. S1: *PMMA parts with capillaries for DoC device. A CNC-based micro-milling machine (CNC Mini-Mill/GX, MINITECH MACHINERY CORP.) with tip sizes of 400 or 1000µm were used to produce the microfluidic device. We milled a cover and a*

base part out of a PMMA sheet with 2mm thickness. The cover has the guidance for the 'INLET' and 'EXIT 2' capillaries as well as the microfluidic channel (500 x 1000 x 90000 µm as HxWxL) for the cell or particle measurements. The hole of the cover as well as the rectangular cuts in the base part are used to hold the capillaries in place and seal the channel using a super glue (ethyl cyanoacrylate 2,2'-methylenebis(6-tert-butyl-4-methylphenol), HENKEL CORP.). Note that the 'INLET' as well as the 'EXIT 2' capillary are circa 2.5mm inserted in the observation channel, resulting in an effective channel length of 8.5cm. The base plate was milled with steps from 50 to 250µm in depth to adjust the mismatch in height of the lateral exit capillary and the observation channel. The 'EXIT 1' capillary is inserted in a 400µm guidance until the observation channel. Cover and base are simply combined by applying temperature (60°C), pressure and 2-propanol (I9516, MERCK KGAA) for 15 minutes.

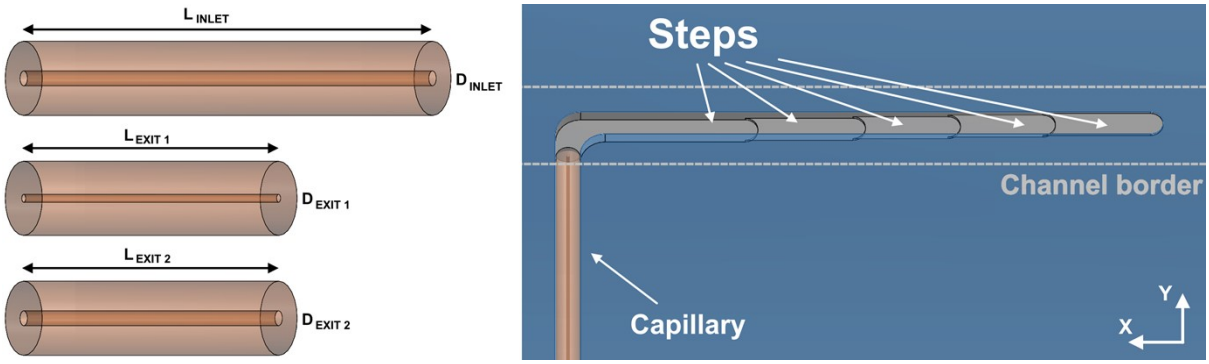

Fig. S2: *Glass capillaries for the microfluidic device and steps in channel. We used three different capillary dimensions and 2 different capillary lengths. The 'INLET' capillary (TSP075375, MOLEX CORP.) was chosen with a dimension of 75µm and length of 34cm. The 'EXIT 1' capillary (TSP040375, MOLEX CORP.) has a diameter of 40µm, while 'EXIT 2' was chosen with 75µm (TSP075375, MOLEX CORP.). Both exit capillaries have a length of 10cm. The 5 steps in the channel bottom have a depth of 50µm each and successive lower the channel bottom in the central part of the channel to a final depth of 750µm. The central line of the lateral capillary -which collect objects from the main-stream is placed at a depth of ~700µm. The step width is 400µm (channel width = 1000µm), while steps start to lower the channel depth 9mm before the lateral exit.*

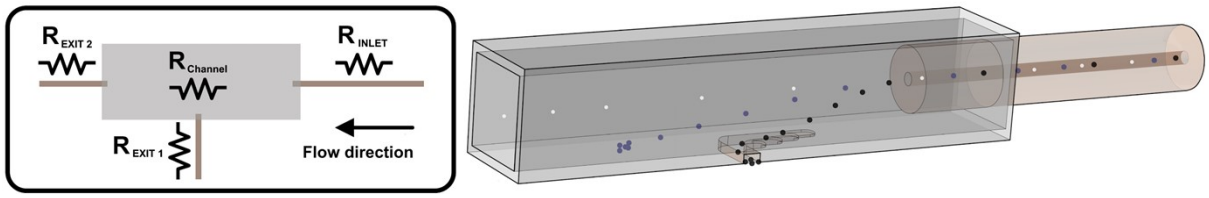

Fig. S3: *Hydraulic resistance of the DoC design. We defined 3 resistances of the capillaries as well as two resistances in the observation channel. One before and one after the lateral exit. The right part of the Fig. illustrates the DoC without lateral and outlet capillaries.*

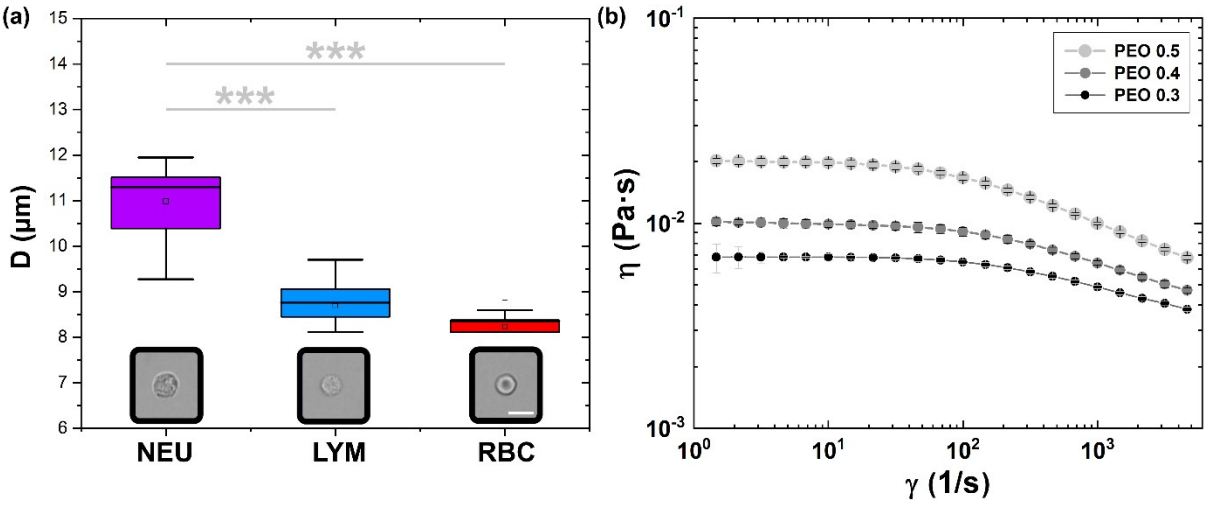

Fig. S4: *Cell dimension and rheological fluid investigations. (a) Cell dimensions were investigated with a bright-field microscope (BX-53, OLYMPUS OPTICAL CORP.) using a x40 magnification combined with a CCD camera (DP21, OLYMPUS OPRICAL CORP.). Neutrophils (NEU), Lymphocytes (LYMPH) and RBCs (RBC) were investigated with ImageJ using a fit ellipse approach. The major axis values for each cell class (n = 9, 24 and 9 for NEU, LYMPH and RBC, respectively) are plotted as well as an illustrative cell image (scale bar = 10µm). (b) Shear-rate-dependent ($\dot{\gamma}$) measurements of the fluid viscosity (η) for PEO dilutions. Rheological data was obtained using a stress-controlled rheometer (MCR302, Anton Paar) with standard cone-plate (diameter of 50mm) geometry.*

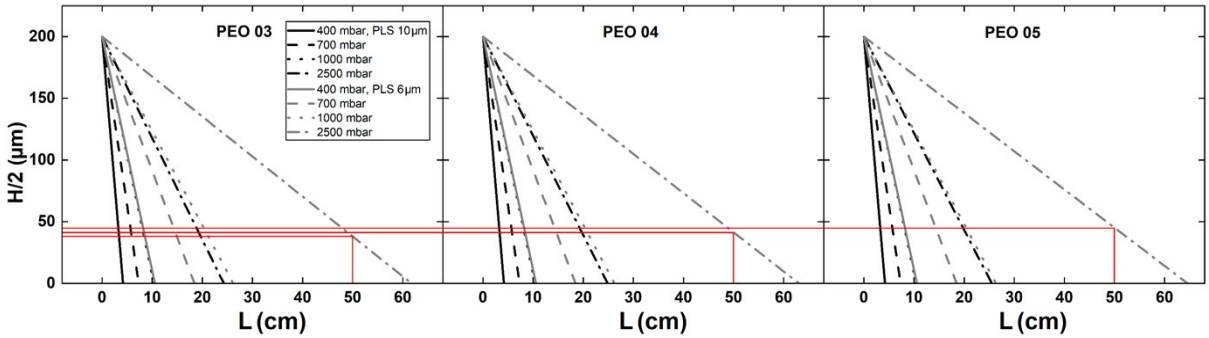

Fig. S5: *Calculation of fall length (L) for calibration beads at different viscoelastic measurement fluids as well as ΔPs. Channel geometry from Fig. S1 was used for the calculations. The red line indicates the Z-position of a particle or cell at measurement position X3 for different viscoelastic fluid conditions. Higher PEO concentrations show higher Z-positions.*

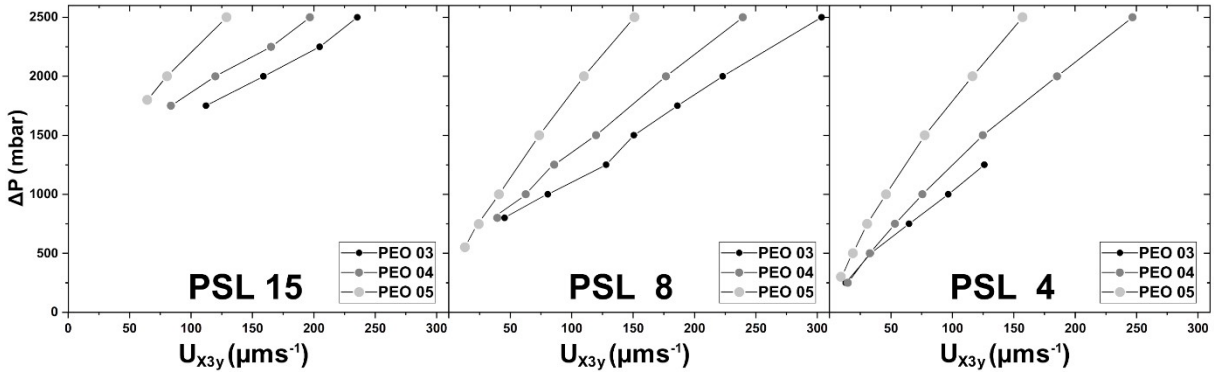

Fig. S6: *We investigated at measurement position X3, how particle size influences the observed particle velocity, which depends on the actual position in the observation channel. Note, different beads dimensions were used for these observations, to show the wide spectrum of particle size that DoC is capable to investigate. At least 10 particle velocities were calculated for each data point. Toward the higher Z-position of particles at higher PEO concentrations, a lower particle velocity for higher PEO concentrations is observed, which is in good agreement with our simulations.*

Table S1: *computed length of sedimentation (Equation 7) is in accordance with the measurements for PSL beads of 10 µm.*

Applied pressure	***L (Equation 7)***	***Experimental L (Fig.2c)***	***Error***
400 mbar	2.2 cm	2 cm	10%
700 mbar	4.1 cm	4 cm	2.5%

Table S2: *Values of density for the investigated PSL sizes compared to values from manufacturer.*

PSL	***Diameter [µm]***	***Density [kg/m³]***	***Density Data Sheet [kg/m³]***
6	6.08	1100	1055
8	8.13	1090	1055
10	10.70	1068	1050
15	15.66	1065	1050

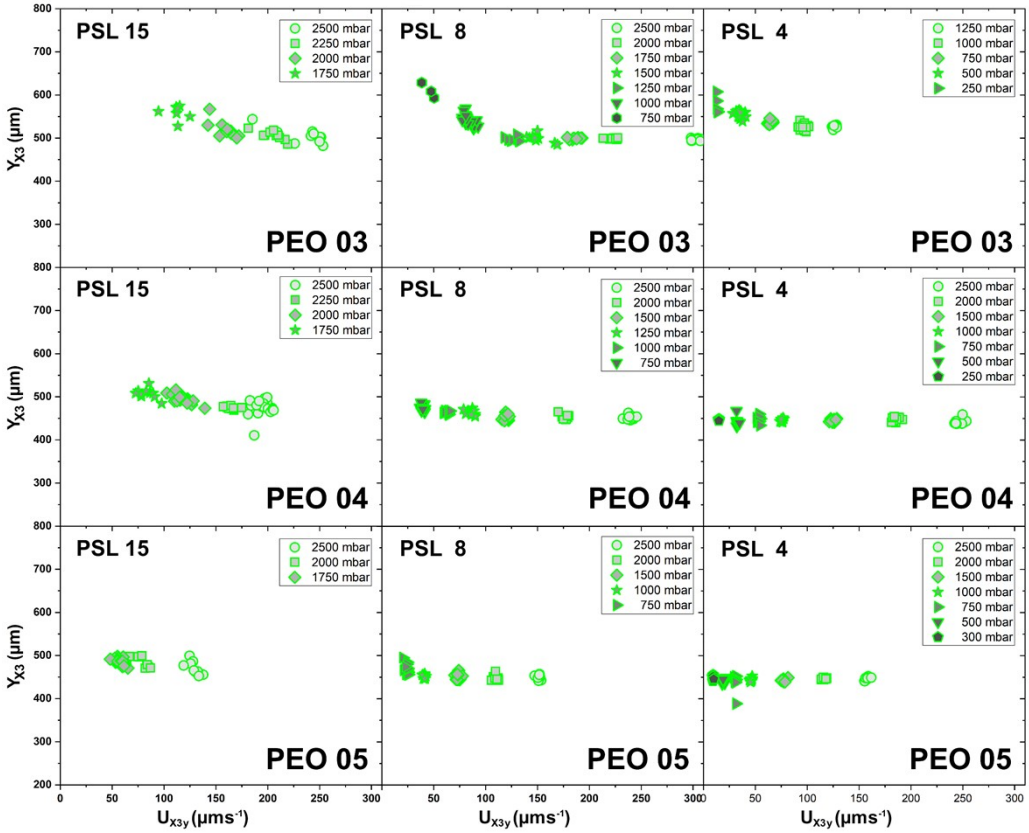

Fig. S7: *The influence of PSL dimension and PEO concentration on the Y-position was investigated. A shift of particles to higher Y-positions at lower particle velocity is evident for lower PEO concentrations.*

Table S3: *Literature values of density for the investigated cell types as well as the major cell components.*

Cell type/structure	***Density (kg/m³)***	***Technique***	***Reference***
RBC*	*1139*	Suspended microchannel resonator	[12]
RBC	*1110*		[13]
RBC	*1099*	Gradient separation	[14]
LYM	*1073-1077*	Ficoll gradient	[15]
LYM	*1080*		[13]
LYM*	*1072*	Gradient separation	[14]
MONO	*1067-1077*	Ficoll gradient	[15]
NEU (low density)	*1081*	Percoll gradient	[16]
NEU (high density)	*1083*	Percoll gradient	[16]
NEU*	*1086*	Gradient separation	[14]
nuclei	*>1300*	Sedimentation through sucrose	[17]
Mitochondria	*1190*	Sedimentation through sucrose	[17]
golgi apparatus	*1060-1100*	Sedimentation through sucrose	[17]
lysosomes	*1210*	Sedimentation through sucrose	[17]
peroxisomes	*1230*	Sedimentation through sucrose	[17]
plasma membranes	*1130*	Sedimentation through sucrose	[17]
nucleic acids, ribosomes	*1600-1750*	Sedimentation through sucrose	[17]
soluble proteins	*1300*	Sedimentation through sucrose	[17]

**Density values for fall length computation.*

Table S4: *Literature values of diameters for the investigated cell types.*

Cell type	***Diameter (µm)***	***Technique***	***Reference***
RBC	*7.5-8.7* *1.7-2.2 (thickness)*	*Extensional Microfluidics*	Diez-Silva et al., 2010
LYM	*8-10*	*Flow Cytometry*	Juan-Manuel Anaya, 2013
NEU	*12-15*	*Light Microscopy*	Ting-Beall et al., 1993

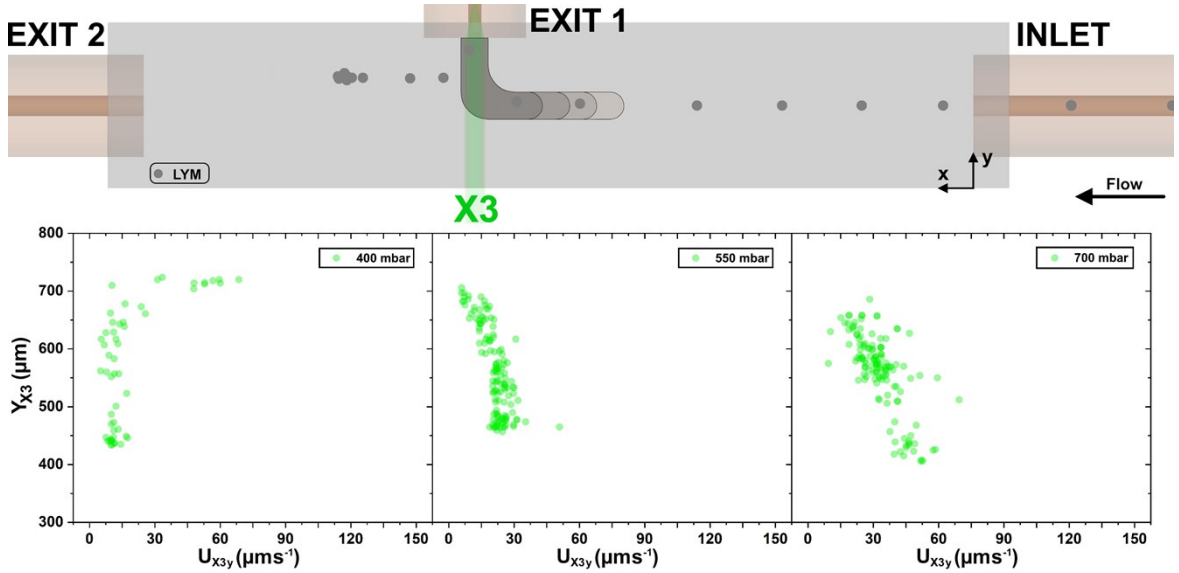

Fig. S8: *Cell tracking outcome for lymphocytes at different ΔP values in measurement position X3. The lowest ΔP indicate a clear increase of cell velocity next at higher distances from the channel centre line (EXIT 1). A ΔP of 550 mbar indicate the lowest cell velocity variance and therefore also the best lateral exit separation outcome. The number of analysed cells for 400, 550 and 700 mbar are 53, 118 and 144 respectively.*

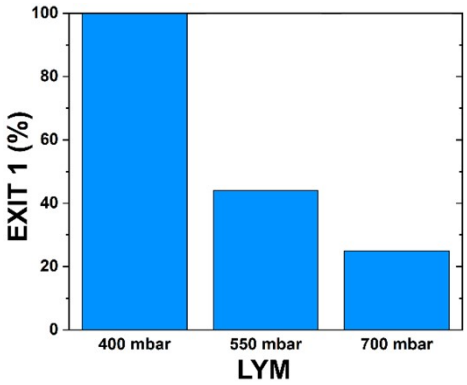

Fig. S9: *Cell separation performance for lymphocytes. A clear separation increase for lower ΔP values is noticed.*

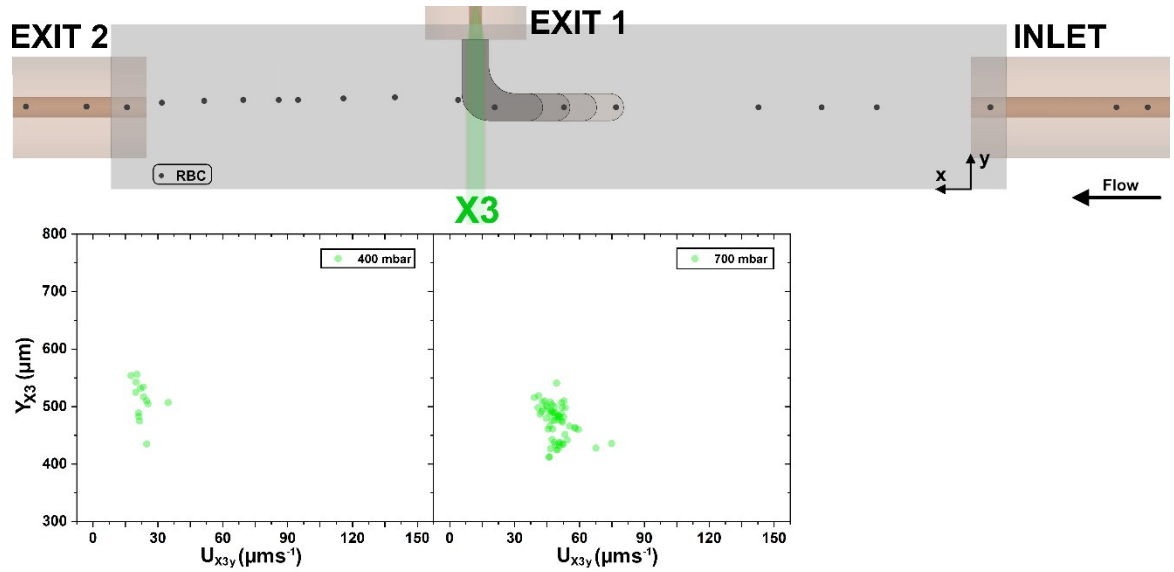

Fig. S10: *Cell tracking outcome for RBCs at different ΔP values in measurement position X3. No significant difference between the different ΔP conditions can be noticed. The number of analysed cells for 400 and 700 mbar are 14 and 61 respectively.*

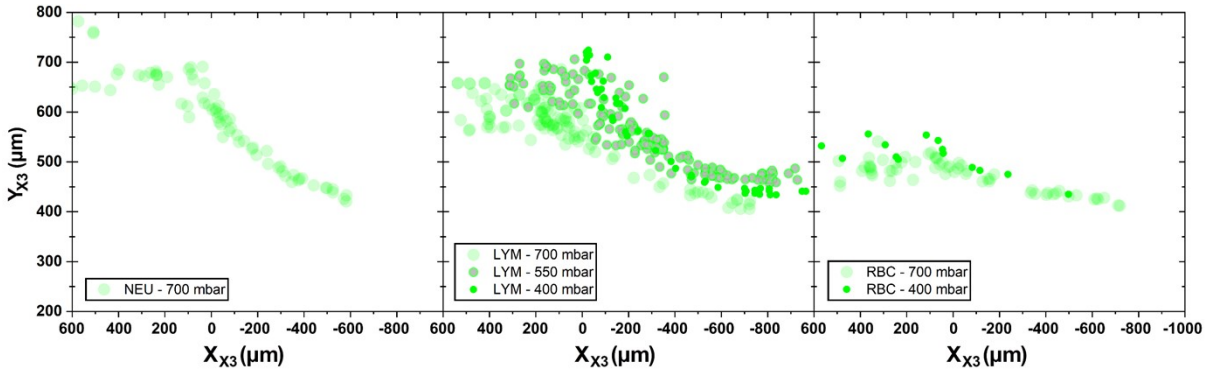

Fig. S11: *The coordinate of tracked cells is presented. Each coordinate represents the average position of both axes (average between first and last tracked coordinate). A clear transition from cell exit to non-exit can be noticed for lymphocytes. The final Y_{X3} position can be interesting for a mass density investigation, because the higher the YX3 position combined with the resulting cell velocity are strong related to the size and density of the investigated cell. The number of analysed NEU are 74 cells. The number of analysed LYM for 400, 550 and 700 mbar are 53, 118 and 144 respectively. The number of analysed RBCs for 400 and 700 mbar are 14 and 61 respectively.*

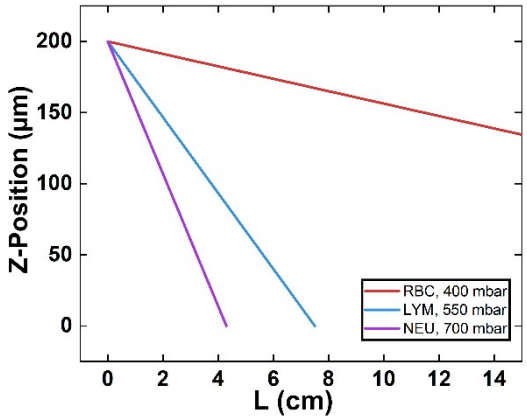

Fig. S12: *The simulated falling length for the investigated cell types. Density values obtained from literature. In more detail, we used density values of 1.072 kg/m³ (LYM), 1.086 kg/m³ (NEU) and 1.099 kg/m³ (RBC). A cell diameter of 8.70 µm (LYM), 10.98 µm (NEU) as well as 8.23 µm (RBC). The applied pressure ΔP is indicated in the legend.*

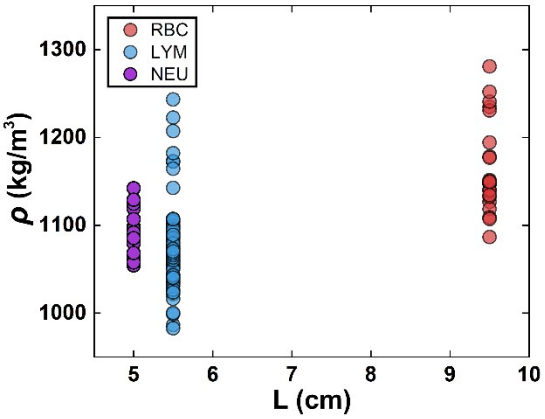

Fig. S13: *Mass density versus fall length for investigated cell types. 22, 78, 15 for RBCs, LYM and NEU respectively. Mean ± std. dev. of ρ: 1159±29.5 kg/m³ for RBCs, 1073±49 kg/m³ for LYM, 1093±27 kg/m³ for NEU.*